Spectroscopy of triply charmed baryons from lattice QCD

M. Padmanath, Robert G. Edwards, Nilmani Mathur, and Michael Peardon (Hadron Spectrum Collaboration)

Phys. Rev. D **90**, 074504 — Published 14 October 2014

DOI: 10.1103/PhysRevD.90.074504

Spectroscopy of triply-charmed baryons from lattice QCD

M. Padmanath,[1,*] Robert G. Edwards,[2,†] Nilmani Mathur,[1,‡] and Michael Peardon[3,§]
(For the Hadron Spectrum Collaboration)

[1] *Department of Theoretical Physics, Tata Institute of Fundamental Research, Homi Bhabha Road, Mumbai 400005, India.*
[2] *Jefferson Laboratory, 12000 Jefferson Avenue, Newport News, VA 23606, USA*
[3] *School of Mathematics, Trinity College, Dublin 2, Ireland*

The spectrum of excitations of triply-charmed baryons is computed using lattice QCD including dynamical light quark fields. Calculations are performed on anisotropic lattices with temporal and spatial spacings $a_t = 0.0351(2)$ fm and $a_s \sim 0.12$ fm respectively and with pion mass of about 390 MeV. The spectrum obtained has baryonic states with well-defined total spin up to $\frac{7}{2}$ and the low-lying states closely resemble the expectation from models with an $SU(6) \times O(3)$ symmetry. Energy splittings between extracted states, including those due to spin-orbit coupling in the heavy quark limit are computed and compared against data at other quark masses.

PACS numbers: 12.38.Gc, 14.20.Mr

I. INTRODUCTION

The charmonium spectrum has been studied in detail both in experiments and theoretical calculations over many years. This has provided crucial input into our understanding of the nature of the strong interaction. In contrast, while charm baryons can provide similar insight, they have not yet been studied so thoroughly. Only a handful of charmed baryons have been discovered and a reliable determination of the quantum number of most of the observed states has not been made [1]. Only very recently have a few excited singly charmed baryons been observed and the discovery status of the doubly charmed baryons remains unsettled. While the SELEX experiment observed doubly charmed $\Xi_{cc}(ccu)$ baryons [2–4], these have not been confirmed either by BABAR [5] or Belle [6]. Along with the well-established triply flavoured $\Delta(uuu)$ and strange $\Omega(sss)$ baryons, QCD predicts similar states built from charm quarks, the triply-charmed baryon, Ω_{ccc}. Such a state has yet to be observed. Beside Ω_{ccc}, QCD also predicts many other triply-charmed baryons, which can be considered as the baryon analogues of charmonia. While it has been pointed out that semileptonic decay processes such as $\Omega_{ccc}^{++} \to \Omega_{sss}^{-} + 3\mu^{+} + 3\nu_{\mu}$ and $\Omega_{ccc}^{++} \to \Omega_{sss}^{-} + 3\pi^{+}$ possibly can offer signature for a "*ccc*" event [7], the production of triply-charmed baryons in current charm factories is difficult (see Refs. [8, 9] for triply-charmed baryon production). However, it is expected that the large statistical sample collected at the LHCb experiment, the PANDA experiment at the FAIR facility, Belle II at KEK and BES III may be able to provide some information on triply-charmed baryons, along with other baryons containing charm quarks.

The triply-charmed baryons may provide a new window for understanding the structure of baryons, as pointed out by Bjorken several years ago [7]. A comprehensive study of the excitation spectra of these states, where the complications of light-quark interaction are absent, can provide information about the quark confinement mechanism as well as elucidating our knowledge about the nature of the strong force by providing a clean probe of the interplay between perturbative and nonperturbative QCD [10]. On the theoretical side, one expects that potential models will be able to describe triply-charmed baryons to a similar level of precision as their success in charmonia. Just as the quark-antiquark interactions are examined in charmonia, these studies will probe the quark-quark interactions in the charm sector. The spectra for triply-charmed baryons have been studied theoretically by non-relativistic [11, 12] and relativistic [13, 14] quark models, quark models in the Faddeev formalism [15], the bag model [16], effective field theory with potential NRQCD [17–20], heavy quark spin symmetry [21], variational method [22], QCD sum rules [23, 24], Regge phenomenology [25] and the one-gluon-exchange model [26]. However, in the absence of any experimental discovery the only way to test these model-dependent as well as perturbative approaches is to compare these with the results from non-perturbative lattice QCD calculations. By using lattice QCD, several calculations have already

*Electronic address: padmanath@theory.tifr.res.in
†Electronic address: edwards@jlab.org
‡Electronic address: nilmani@theory.tifr.res.in
§Electronic address: mjp@maths.tcd.ie

been performed to compute the ground state triply-charmed baryon, $\Omega_{ccc}(J^P = \frac{3}{2}^+)$, including quenched [27] as well as full QCD [28–32].

A quantitative description of the spectra of triply-charmed baryons using a non-perturbative method such as lattice QCD is thus important for a number of reasons. Firstly, as mentioned above, it will be interesting to compare the spectra of triply-charmed baryons computed from a first principles method to those obtained from potential models which have been very successful for charmonia. Secondly, all results from such first principles calculations will be predictions and thus naturally can provide crucial inputs to future experimental discovery. Given this significance of triply-charmed baryons, it is desirable to study these states comprehensively using lattice QCD. All previous lattice calculations have studied only the $\Omega_{ccc}(J^P = \frac{3}{2}^+)$ ground state. However, it is expected that more information about interactions between multiple charm quarks can be obtained by computing the excited state spectra of $\Omega_{ccc}(J^P = \frac{3}{2}^+)$ baryons, including in particular the spin-dependent energy splittings, as well as by studying similar spectra for other triply-charmed baryons with all spin and parity combinations. In this work, we make the first attempt towards this goal and compute the excited state spectra of triply-charmed baryons using dynamical lattice QCD. The ground states for each spin-parity channel up to spin 7/2 are computed along with a number of their excited states and several spin-dependent energy splittings. Similar studies of singly and doubly-charmed baryons will be reported in subsequent publications.

We use a well defined procedure developed and employed extensively for extracting excited states for light mesons [33–35], mesons containing charm quarks [36, 37], and light and strange baryons [38–40]. This method uses anisotropic lattice configurations with the light quark dynamics included [41, 42]. The anisotropic discretisation helps us to obtain better resolution of the correlation functions, which is very helpful for the extraction of excited states. Furthermore, we construct a large set of baryonic operators in the continuum and then subduce them to various lattice irreducible representations to obtain lattice operators [38]. These operators transform as irreducible representations (irreps) of $SU(3)_F$ symmetry for flavour, $SU(4)$ symmetry for Dirac spins of quarks and $O(3)$ symmetry for orbital angular momenta. Finally, using a novel technique called "distillation" [43], correlation functions of these operators are computed and the variational method is utilized to extract excited energies as well as to reliably determine the spins of these states.

The layout of the remainder of the paper is as follows. In the next section, we describe the details of our numerical methods mentioning first the details of lattices used and then the construction of the lattice interpolating operators in subsection IIB. In subsection IIC, we detail the generation and analysis of baryon correlation functions by distillation and variational methods and then in IID we discuss our procedure of identifying the continuum spins of the extracted states; subsection IIE discusses about the lattice artefacts related to this work. In section III we present our results and give details of energy splittings in subsection IIIA. Finally, a summary of the work is presented in section IV.

II. LATTICE METHODOLOGY

In this section, the details of our Monte Carlo calculation of triply charmed baryon excitations using lattice QCD are described. In recent years the Hadron Spectrum Collaboration has exploited a dynamical anisotropic lattice formulation to extract highly excited hadron spectra. In this approach a lattice with a much finer temporal spacing than in the spatial directions is employed. The high temporal resolution means many time slices are available to compute the signal for highly excited states which decay very rapidly at large Euclidean time separations leading to a increase in the noise-to-signal ratio. The anisotropic lattice achieves this resolution while avoiding the computational cost which would come from reducing the spacing in all directions.

A. The lattice action

The tree-level Symanzik-improved gauge action and the anisotropic Shekholeslami-Wohlert fermion action with tree-level tadpole improvement and three-dimensional stout-link smearing of gauge fields are used. More details of the formulation of actions as well as the techniques used to determine the anisotropy parameters can be found in Refs. [41, 42].

Lattice size	$a_t m_\ell$	$a_t m_s$	N_{cfgs}	m_π/MeV	m_K/m_π	$a_t m_\Omega$
$16^3 \times 128$	-0.0840	-0.0743	96	391	1.39	0.2951(22)

TABLE I: Properties of the gauge-field ensembles used. N_{cfgs} is the number of gauge-field configurations.

The lattice action parameters of the gauge-field ensembles used this work are given in Table I. As mentioned in Ref. [38], the temporal lattice spacing a_t was determined by equating the Ω-baryon mass measured on these ensembles $a_t m_\Omega = 0.2951(22)$ with the physical value, $m_\Omega = 1672.45(29)$ MeV. This leads to $a_t^{-1} = 5.67(4)$ GeV and with an anisotropy of close to 3.5, $a_s = 0.12$ fm. This gives a spatial extent of about 1.9 fm, which should be sufficiently large for a study of triply-charmed baryons.

The details of the charm quark action used for this study are given in Ref. [36]. The action parameters for the charm quark are obtained by ensuring the mass of the η_c meson takes its physical value and its dispersion relation at low momentum is relativistic. As mentioned in [36], it is expected that the effects due to the absence of dynamical charm quark fields in this calculation will be small.

B. Baryon operator construction

We follow the same methods described in Ref. [38] for the construction of baryon interpolating operators on the lattice. Baryons are colour singlets made of three quarks and so have anti-symmetric wave functions in colour space. Since they are fermions, their interpolating operators excluding the colour part should be totally symmetric combinations of all the quark labels representing flavour, spin and the spatial structure. Our construction of baryon interpolating operators proceeds in two stages; first, a set of continuum operators with well-defined continuum spin is defined. These operators are then subduced into irreducible representations of the double-cover octahedral group.

The overall spin and parity of a continuum baryon interpolating operator can be found by decomposing it into a combination of three components;

$$O^{[J^P]} = [\mathcal{F}_{\Sigma_F} \otimes \mathcal{S}_{\Sigma_S} \otimes \mathcal{D}_{\Sigma_D}]^{J^P}, \tag{1}$$

where $\mathcal{F}$, $\mathcal{S}$ and $\mathcal{D}$ represent flavour, Dirac spin and spatial structure respectively while the subscripts Σ_i specify the permutation symmetry in the respective subspaces. The details of these permutation symmetries and their combinations are given in Refs. [38, 40]. After combining them together, we get interpolating fields with specific spin and parity which are overall symmetric under permutations. The flavour combination $\mathcal{F}_{\Sigma_F}$ of triply-charmed operators must be totally symmetric and is the same as that of the $I_Z = \pm 3/2$ part of the Δ and the Ω baryon operators. Consequently the remaining spin and spatial part must be combined together in a symmetric combination to form an overall symmetric interpolating operator. The spin symmetry combinations $\mathcal{S}_{\Sigma_S}$ in Dirac space can be obtained by combining the ρ and σ spins for a quark field $\psi^\mu = q^\rho_\sigma$, as explained in Ref. [38]. Only creation operators formed from the upper two components of the four-component Dirac spinor appear at leading order in a velocity expansion. Those based on the lower components of Dirac spinors are relativistic.

The spatial symmetry combinations $\mathcal{D}_{\Sigma_D}$ depend on the gauge covariant derivatives acting on the three quark fields. As in our previous studies [38, 40], we include up to two covariant derivatives. These are combined to transform irreducibly with orbital angular momentum, L, giving access to $L = 0, 1$ and 2. Without derivatives, only the totally symmetric Dirac spin structure is allowed. The single derivative structures can have mixed symmetry or mixed antisymmetry and hence they can only be combined with Dirac spin structures with mixed symmetry and mixed antisymmetry respectively. With up to one derivative it is possible to construct operators with spins up to $\frac{3}{2}$ while for baryons with flavour-mixed symmetry it is up to $\frac{5}{2}$. However, two derivative projection operators can be combined with all spin symmetry combinations $\mathcal{S}_{\Sigma_S}$ in Dirac space which enables states with spins up to $\frac{7}{2}$. In Table II, we show allowed spin-parity patterns of operators using the upper quark spinors combined with up to two covariant derivatives. Note that with the non-relativistic Dirac spin components alone, it is not possible to construct a negative parity state beyond spin $\frac{3}{2}^-$ even with operators that include two derivatives. This limited the extraction of spin $\frac{5}{2}^-$ and spin $\frac{7}{2}^-$ states in Ref. [48]. Use of relativistic operators along with non-relativistic ones enable us to extract these negative parity states along with more excited states.

With two derivatives, a subset of operators with $L = 1$ in mixed-symmetric and mixed-antisymmetric combinations [39] are identified as hybrid operators because they vanish in the absence of a gluon field. Note that a colour-singlet object $[(qqq)_{8_c} G_{8_c}]_{1_c}$ can be constructed through a combination of three quarks in a colour octet with a gluon field, G. Table II shows the pattern of states expected to be created by two-derivatives operators built from non-relativistic quark spinors. As will be observed later, operators which incorporate the gluon field-strength tensor are essential in obtaining some states in the spectrum.

To define a creation operator that respects the symmetries of the lattice, continuum operators with definite spin and parity are subduced into the irreps of the cubic group. The three irreps of the double-valued representations of the octahedral group for half-integer spins are G_1, G_2 and H. The details of this subduction procedure was discussed in Ref. [38]. After completing the subduction procedure, the number of operators used for this study are shown in Table III. In each irrep, the same number of operators for both positive and negative parities, denoted by the subscript

			$N(J^P)$					
N_D	L	S	$\frac{1}{2}^+$	$\frac{3}{2}^+$	$\frac{5}{2}^+$	$\frac{7}{2}^+$	$\frac{1}{2}^-$	$\frac{3}{2}^-$
0	0	$\frac{3}{2}$		1				
1	1	$\frac{1}{2}$					1	1
2	0	$\frac{1}{2}$	1					
2	0	$\frac{3}{2}$		1				
2	**1**	$\mathbf{\frac{1}{2}}$	**1**	**1**				
2	2	$\frac{1}{2}$		1	1			
2	2	$\frac{3}{2}$	1	1	1	1		

TABLE II: The number of operators of a given J^P that can be constructed from up to two derivatives acting on non-relativistic quark spinors. N_D indicates the number of covariant derivatives, S indicates the total spin of the quarks and L indicates the total orbital angular momentum. The row indicated in bold face contains the two-derivative "hybrid" operators, which vanish in the absence of a gluon field.

g and u, respectively are used. This table also gives the number of operators made exclusively from non-relativistic quark spinors (NR) and those hybrid operators which vanish in the absence of a gluon field.

We have followed the same naming convention as Ref. [38]. Since there are only charm valence quarks in this calculation we do not refer to flavour and name an operator according to its spin and spatial structure. For example, in the operator $O = [(\frac{3}{2}{}^+_{1,S}) \otimes D^{[2]}_{L=2,S}]^{\frac{7}{2}} H_{g1}$, the label $(\frac{3}{2}{}^+_{1,S})$ indicates the quark spins are combined to form the first (1) embedding of the H_g (3/2) irrep in the symmetric (S) combination, $D^{[2]}_{L=2,S}$ represents two covariant derivatives with two units of angular momentum in the symmetric combination, the $^{\frac{7}{2}}$ part of the name indicates the continuum spin $J = 7/2$ and H_{g1} indicates the lattice operator transforms as the first row of the subduced irrep H_g.

	G_1		H		G_2	
	g	u	g	u	g	u
Total	20	20	33	33	12	12
Hybrid	4	4	5	5	1	1
NR	4	1	8	1	3	0

TABLE III: The number of lattice operators obtained after subduction to various irreps of operators with up to two covariant derivatives. The number of non-relativistic (NR) and hybrid operators for each irreps and for both parities are given.

C. Variational analysis of correlation functions

We employ a variational method to extract the spectrum of baryon states from the matrix of correlation functions calculated by using the large basis of interpolating operators described above. For operators i and j, in a given irrep Λ, we calculate the matrix of correlation functions

$$C^{\Lambda}_{ij}(t_f - t_i) = \langle 0|\bar{O}_i(t_f) O_j(t_i)|0\rangle. \tag{2}$$

between a baryon creation operators at time t_i and an annihilation operator at time t_f. An efficient way to construct this correlation matrix for the large basis of interpolating operators utilized in this work is through the *distillation method*, detailed in Ref. [43] and utilized in various calculations by the collaboration. Distillation is a smearing method that defines a linear smoothing operator with support only in a small space of physically relevant vectors. As with other recent calculations by the collaboration, we use the low-lying eigenvectors of the gauge-covariant three-dimensional Laplacian in this calculation. The correlation function of Eq. 2 then factorises, enabling efficient computation of all elements of the matrix. The distillation method is useful for these calculations since it provides a technique to determine the full matrix of correlation functions for any number of *smeared* operators at both source and sink. For

this work, the distillation method was realized by constructing the smearing operator from the lowest 64 eigenvectors of the Laplacian. Correlation functions are then constructed using a set of four time sources per gauge configuration.

The variational method enables a reliable extraction of the spectrum beyond the ground state. The method [46, 47] proceeds by solving a generalized eigenvalue problem of the form

$$C_{ij}(t)v_j^n = \lambda_n(t,t_0)C_{ij}(t_0)v_j^n, \tag{3}$$

where v^n is the n-th eigenvector and the eigenvalues, $\lambda_n(t,t_0)$ are termed the *principal correlators* and obey

$$\lim_{t-t_0\to\infty} \lambda_n(t,t_0) = e^{-E_n(t-t_0)} \tag{4}$$

with E_n the energy of the n-th excited state. An appropriate reference time-slice t_0 is chosen for diagonalization as described in Refs. [33, 34, 49], which corresponds to a minimum of a χ^2-like quantity as defined in Ref. [49]. We extract the energy of a state by fitting the dependence of λ_n on $t-t_0$ to the form,

$$\lambda_n(t,t_0) = (1-A_n)e^{-m_n(t-t_0)} + A_n e^{-m'_n(t-t_0)}, \tag{5}$$

with three fit parameters m_n, m'_n and A_n. As with our previous studies, we find that allowing a second exponential stabilizes the fits and the resulting second exponential decreases rapidly with large t_0. All the excited states in our fits are found to be less than the second exponential m'_n. In Figure 1, we plot some examples of fits to the principal correlators in irrep H_g, where the fitted states will be identified with $J^P = \frac{3}{2}^+$. The fits approach the constant value, $1-A_n$, for large t, and they approach one if a single exponential dominates. This is seen to be the case for most of our fits. In Table IV we show fit results for the lowest three states in each irrep. While fitting principal correlators we used a standard χ^2 minimization procedure incorporating the measured data covariance.

Irrep	positive parity			negative parity		
	$a_t\ m_n$	Range	χ^2/DOF	$a_t\ m_n$	Range	χ^2/DOF
G_1	0.9460 (23)	[3-22]	1.30	0.8970 (16)	[4-22]	1.44
	0.9470 (24)	[3-22]	0.94	0.9832 (54)	[4-22]	0.77
	0.9505 (23)	[3-22]	0.62	0.9866 (76)	[4-22]	2.54
H	0.8345 (11)	[4-22]	1.49	0.8977 (23)	[4-22]	0.97
	0.9315 (55)	[14-22]	1.55	0.9558(259)	[5-20]	1.20
	0.9513 (22)	[3-22]	1.62	0.9920 (53)	[4-22]	0.76
G_2	0.9523 (18)	[1-22]	1.67	0.9189(217)	[5-22]	1.36
	0.9524 (25)	[3-22]	1.38	0.9812(117)	[12-22]	1.96
	0.9529 (32)	[4-22]	1.56	0.9977 (55)	[4-22]	0.88

TABLE IV: Fit results from principal correlators of the lowest three states in all the irreps.

D. Rotational symmetry and continuum spin identification

One goal of lattice calculations such as this one is to ensure that any states identified can be assigned continuum quantum numbers in a reliable way. As the continuum limit is taken, rotational symmetry should be restored. The use of smeared fields in construction operators should to help make this restoration more directly observable.

With the aim of making a more direct link with physical quantum numbers, operators were constructed first in the continuum and then subduced onto the lattice irreps. Therefore, it is useful to determine whether these lattice operators exhibit a remnant of the continuum rotational symmetry on the lattice. To check this, Figure 2 shows the correlation function in the H_g irrep at time-separation $5a_t$ after normalizing using $C_{ij}/\sqrt{C_{ii}C_{jj}}$. The choice of time-separation here is arbitrary, with alternatives giving similar pictures. We do not use this figure for spin identification. The normalization ensures all the diagonal entries are unity, while cross correlations are always less than 1. Various operators are represented by the following abbreviations: 'r' indicates relativistic quark spinor components are used while 'nr' indicates non-relativistic spinor only. 'h' denotes hybrid operators and 'nh' indicates non-hybrid. There are 33 operators used in this irrep, including operators up to two derivatives. The solid lines divide these operators subduced from continuum spins $\frac{3}{2}$, $\frac{5}{2}$ and $\frac{7}{2}$, and the dashed lines are used for separating operators defined above with

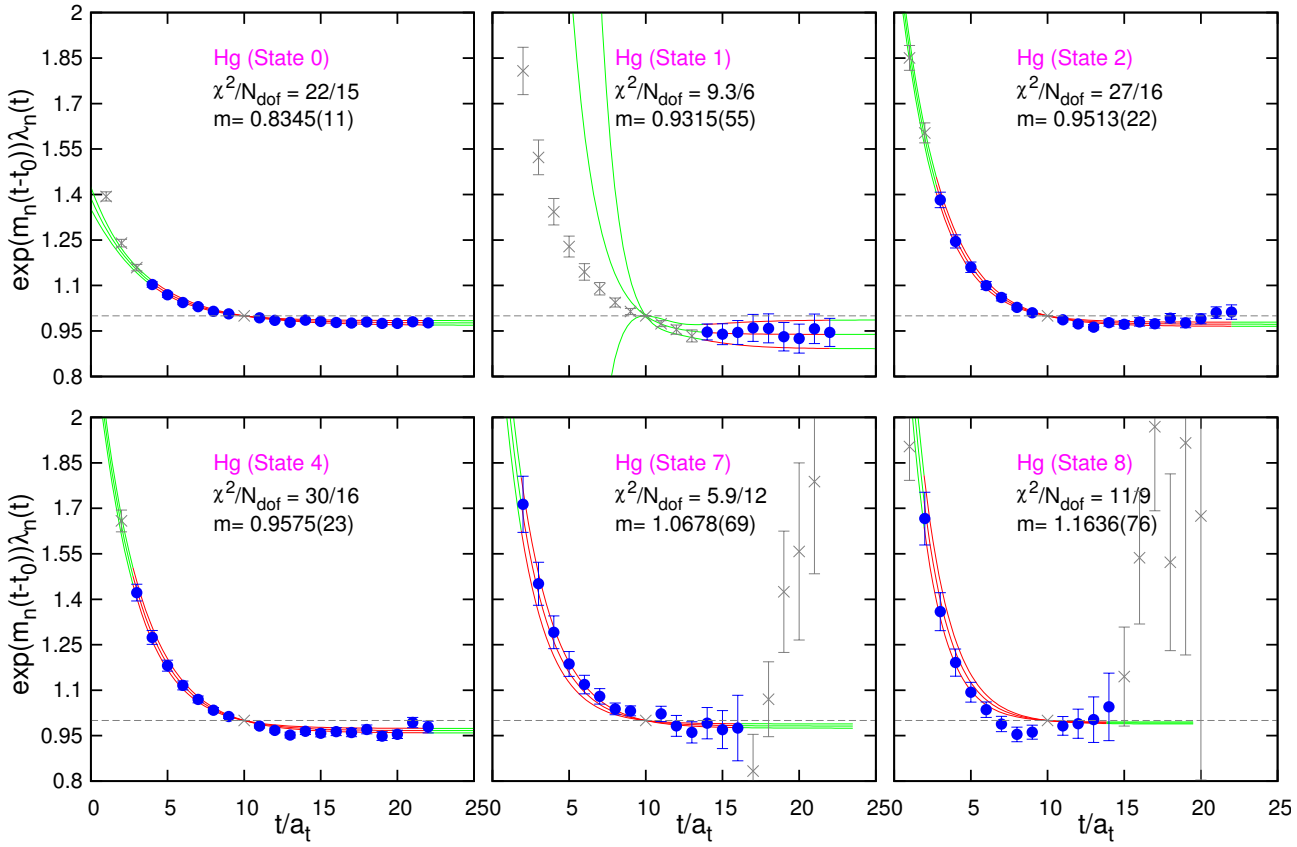

FIG. 1: Principal correlator fits for six states in irrep H_g that are identified as $J^P = 3/2^+$. Fits are obtained using eq. (5). Data points are obtained from $e^{m_n(t-t_0)}\lambda_n(t)$ and the lines show the fits and one sigma-deviation according to the fitting form $e^{m_n(t-t_0)}\lambda_n(t) = 1 - A_n + A_n e^{-(m'_n - m_n)(t-t_0)}$, with $t_0 = 10$; the grey points are not included in the fits.

various abbreviations. The matrix is seen to be almost block diagonal in the continuum spin label. A similar pattern is also observed for light and strange baryons [40] and our result for triply-charmed baryons also suggests that after the subduction a remarkable degree of rotational symmetry remains. Similar block-diagonal matrices of correlation functions are also observed within other irreps. The approximate block-diagonal structure of these matrices gives confidence in our ability to make unambiguous spin-identification for triply-charmed baryons.

From this figure, we can also identify the mixing between different operators. For example, it is evident from Figure 2 that there is strong mixing between 'nr-nh' and 'r-nh' type operators and comparatively weak mixing between 'h' and 'nh'-type operators. As was observed in Ref. [48], we also found additional suppression of mixing for operators with a given J, but with different L and S, compared to those with the same J, as well as the same L and S. For example, for the operators $O_1 = [(\frac{3}{2}^+_{1,S}) \otimes D^{[0]}_{L=0,S}]^{\frac{3}{2}} H_{g1}$ and $O_2 = [(\frac{3}{2}^+_{1,S}) \otimes D^{[2]}_{L=0,S}]^{\frac{3}{2}} H_{g1}$ which both have $J = 3/2, L = 0, S = 3/2$ the matrix element $M_{12} = C_{12}/\sqrt{C_{11}C_{22}} = 0.99$. On the other hand, the mixings of these operators with $O_3 = [(\frac{3}{2}^+_{1,S}) \otimes D^{[2]}_{L=2,S}]^{\frac{3}{2}} H_{g1}$ which has $J = 3/2, L = 2, S = 3/2$ are $M_{13} = 0.0026$ and $M_{23} = 0.0031$. This suppression of mixing is however evident only for the non-relativistic operators. We found that for some relativistic operators mixing enhance between operators with same J but different L and S, compared to those with same J, L and S.

To identify the spin of a state we followed the same method detailed in Ref [49] and used in the calculations of light mesons [33–35], baryons [38, 40], charm mesons [36] as well as heavy-light mesons [37]. The main ingredient is the *overlap-factor*, Z^n_i, of an operator, O_i, to a state, n, which we define as, $Z^n_i \equiv \langle n|O^\dagger_i|0\rangle$. It is possible to show that these overlap factors enter in the spectral decomposition of the matrices of the correlation functions as,

$$C_{ij}(t) = \sum_n \frac{Z^{n*}_i Z^n_j}{2m_n} e^{-m_n t}. \tag{6}$$

Furthermore, one can use the orthogonality for the eigenvectors $v^{n\dagger}C(t_0)v^m = \delta^{n,m}$ to show that the overlap factors can be obtained from the eigenvectors from the relation

$$Z_i^n = \sqrt{2m_n}e^{m_n t_0/2} v_j^{n*} C_{ji}(t_0). \tag{7}$$

As in previous studies, we utilize these overlap factors for spin identification. Figure 3 shows a histogram of these factors for a number of operators onto some of the lower-lying states in each of the lattice irreps. The factors presented in this figure are normalized according to $\frac{Z_i^n}{max_n[Z_i^n]}$ such that the largest overlap across all states for a given operator is unity. The figure shows clearly that for each state, operators coming from a single set subduced from a continuum spin dominate. This gives us confidence in the spin assignment for the triply-charmed baryons.

As in Ref. [40], one can also show a "matrix" plot to depict the dominant contribution to each state from all operators. Figure 4 and Figure 5 show examples for the G_{1g} and H_g irreps where the horizontal axis corresponds to the operator index, while the vertical location indicates the different states obtained in the fitting procedure. Solid lines between columns are used to distinguish operators subduced from different continuum spins while dashed lines separate operators of different types in a given spin. Figure 4 shows states 2 and 8 predominantly overlap with spin $\frac{7}{2}^+$ operators and hence can be identified as $J^P = \frac{7}{2}^+$ states. For all other fitted states, dominant overlaps are from spin $\frac{1}{2}^+$ operators. However, in order to confirm the reliability of the identification of a state with a given spin one has to compare the magnitudes of overlap factors of one operator which is subduced into different irreps, which will be discussed later.

These plots give some information on the structure of a state, in particular the type of operators from which it is constructed. For example, states 2 and 8 in G_{1g}, which are identified as $\frac{7}{2}^+$ states, have predominant overlap to non-relativistic non-hybrid and relativistic non-hybrid operators respectively. Similarly, state 4 overlaps mainly with relativistic non-hybrid operators. Strong hybrid content was similarly observed in a number of states. It is to be noted

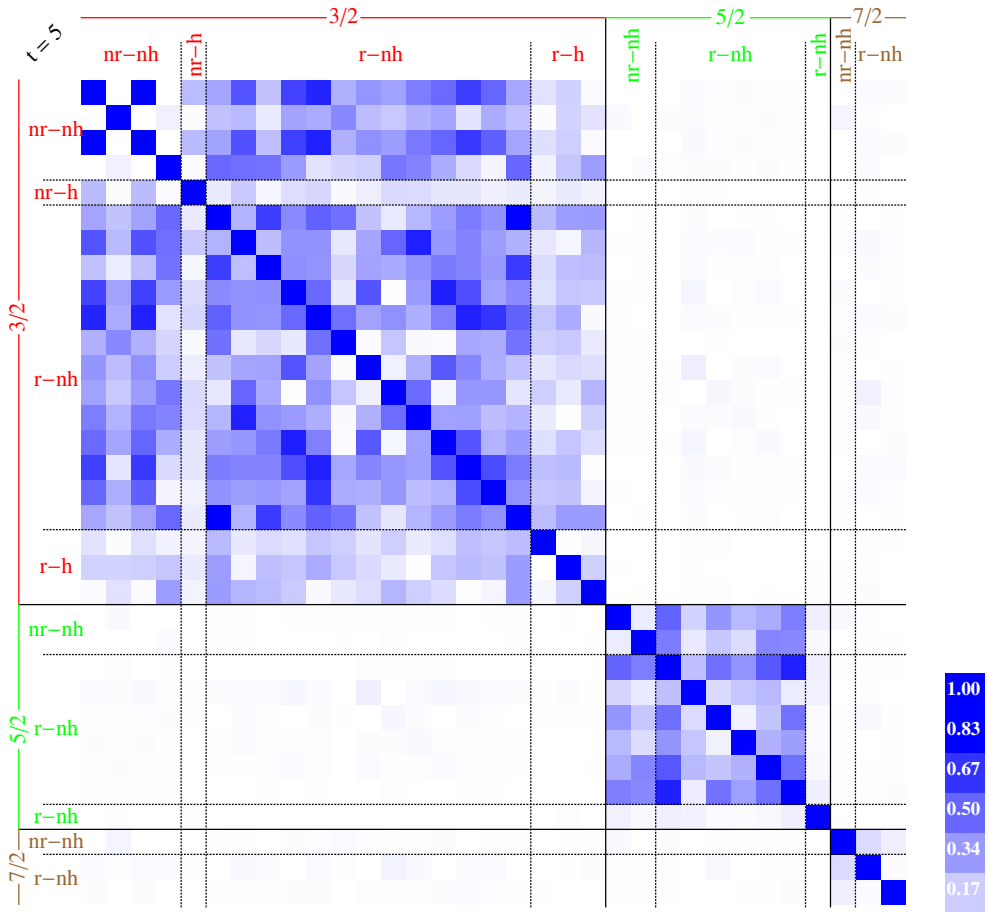

FIG. 2: A normalized correlation matrix, $C_{ij}/\sqrt{C_{ii}C_{jj}}$, at a given time slice at $t/a_t = 5$ for the H_g irrep. Operators are ordered such that those subduced from spin 3/2 appear first followed by spin 5/2 and then spin 7/2.

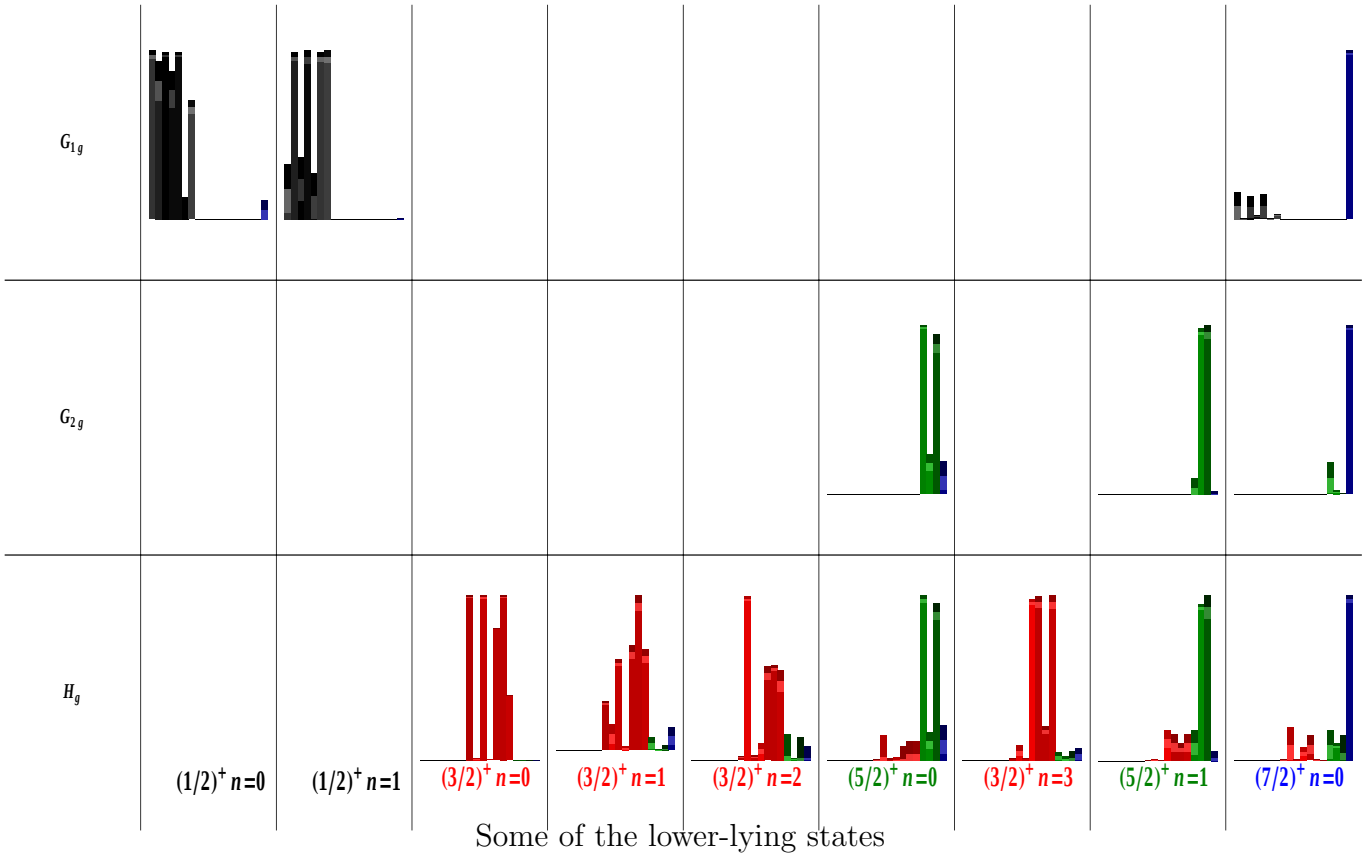

FIG. 3: Histograms of the normalized overlap factor, Z of a set of operators onto some of the lower-lying states in each lattice irrep. The overlaps shown are weighted $\frac{Z_i^n}{max_n[Z_i^n]}$, such that the largest normalised value across all states for a given operator is unity. Various operators are depicted in each state however, due to the large basis size, their names are not shown here. Black bars correspond to spin-1/2 state, red for spin-3/2, green for spin-5/2 and blue represents spin-7/2 states. Lighter and darker shades at the top of each bar represent the one-sigma statistical uncertainty.

from these figures that hybrid operators contribute predominantly to high-lying states in our observed spectrum.

To identify a spin contained within a single irrep is relatively easy. For example, by studying the overlap factors shown in the histogram and matrix plots spin-$\frac{1}{2}$ and spin-$\frac{3}{2}$ states are clearly identified. However, spin-$\frac{5}{2}$ and spin-$\frac{7}{2}$ states appear in multiple lattice irreps and so more information is crucial. In these cases, an operator can be subduced to various irreps but in the continuum limit, overlap factors of a continuum operator with a particular state obtained from various cubic irreps should be almost the same. For example, the spin-7/2 continuum operator, $[(3/2^+)_{1,S} \otimes D^{[2]}_{L=2S}]^{\frac{7}{2}^+}$, can be subduced to irrep G_{1g}, H_g as well as to G_{2g}. However, it is expected that at a finite lattice spacing for a particular spin $\frac{7}{2}^+$state which is near degenerate over these irreps, overlap factors of the above operator to that state would also be degenerate. This near degeneracy of overlap factors identifies this state as spin-$\frac{7}{2}^+$ state. In Figure 6 we compare a selection of Z-values for states conjectured to be $J = \frac{5}{2}^+$ (top two plots), $\frac{5}{2}^-$ (middle two plots), $\frac{7}{2}^+$ (bottom left) and $\frac{7}{2}^-$ (bottom right) which can be subduced to different irreps. The values of Z obtained for a given operator from different irreps are found to be consistent, or have very small deviations in high-lying states which gives confidence in the spin interpretation. Deviations may be due to small remaining renormalisation or discretisation artefacts.

E. Investigating lattice artefacts

For a simulation carried out at a finite lattice cut-off, the results obtained will differ from their continuum counterparts and the difference can be understood in a Symanzik expansion in powers of the lattice spacing. Usually, the best means of removing these artefacts is to perform calculations at a range of lattice spacings and to use the expansion to

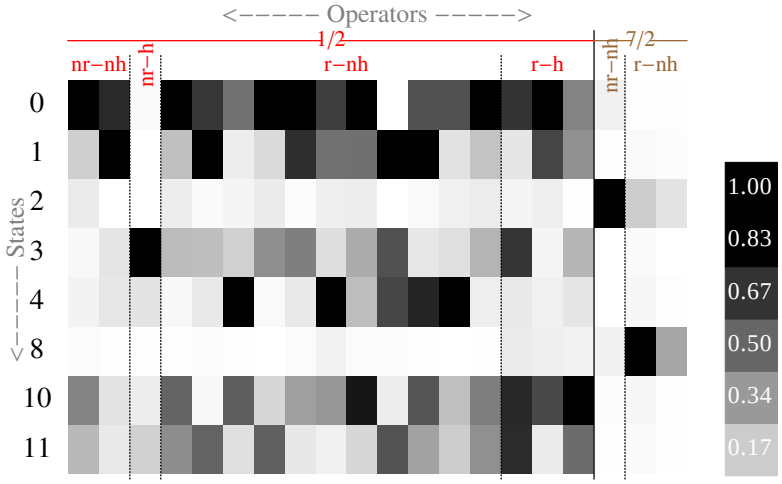

FIG. 4: "Matrix" plot of values of overlap factor, Z_i^n, of an operator i to a given state n, as defined by eq. (7). Z_i^n are normalized according to $\frac{Z_i^n}{max_n[Z_i^n]}$, so that for a given operator the largest overlap across all states is unity. The normalized magnitudes of various operator overlaps to states in the G_{1g} irrep are shown. Darker pixel indicates larger values of the operator overlaps as shown in the adjacent legend. Various type of operators, for example, non-relativistic (nr) and relativistic (r) operators, as well as hybrid (h) and non-hybrid (nh) operators are indicated by column labels. In addition, the continuum spins of the operators are shown by 1/2 and 7/2. State 0, the ground state, and excited states 1, 3, 4, 10 and 11 are identified with $J^P = \frac{1}{2}^+$ from the overlap to various types of operators according to pixel strength. States 2 and 8 are identified as $J^P = \frac{7}{2}^+$ states with the predominant overlap to non-relativistic non-hybrid and relativistic non-hybrid operators respectively.

extrapolate to vanishing lattice spacing. In this study, we do not have sufficient data to carry out this extrapolation.

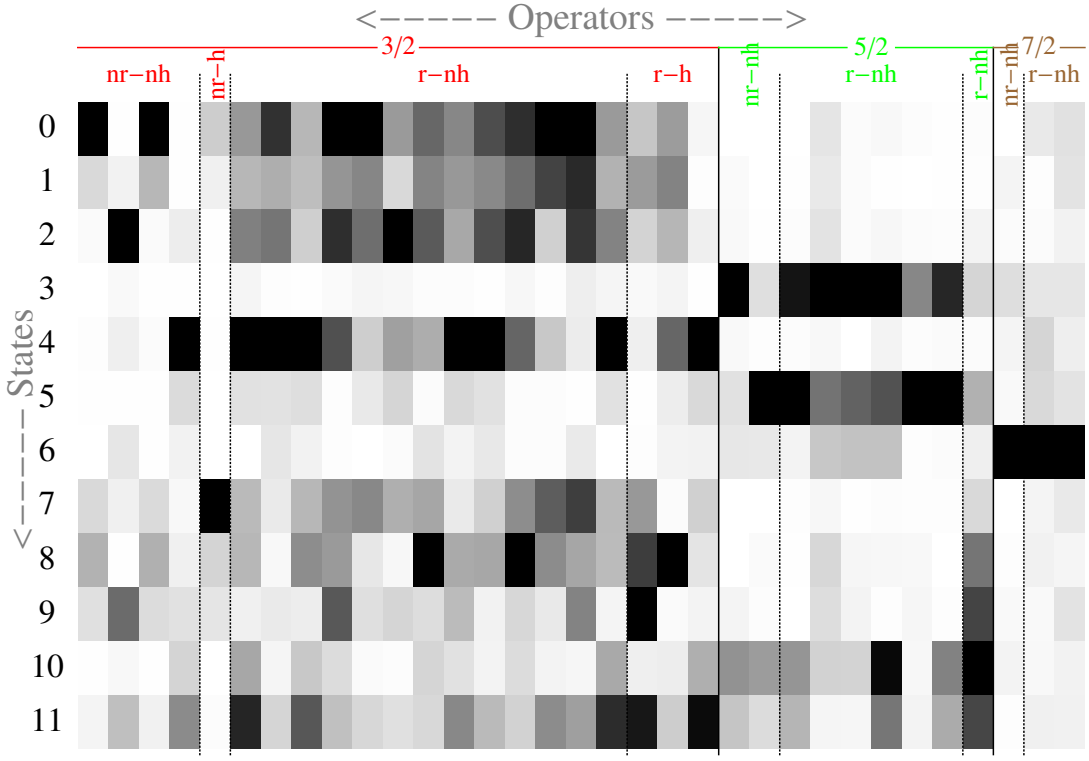

FIG. 5: Same "matrix" plot, as Figure 4, for the H_g irrep. Here one can associate state 6 with quantum number $J^P = \frac{7}{2}^+$, the states 3, 5 and 10 with $J^P = \frac{5}{2}^+$, and the rest with $J^P = \frac{3}{2}^+$. The states 7 and 9 are predominantly hybrid in nature, while states 4, 8 and 10 are found to have substantial overlap with non-hybrid operators. Pixel legend is same as in Figure 4.

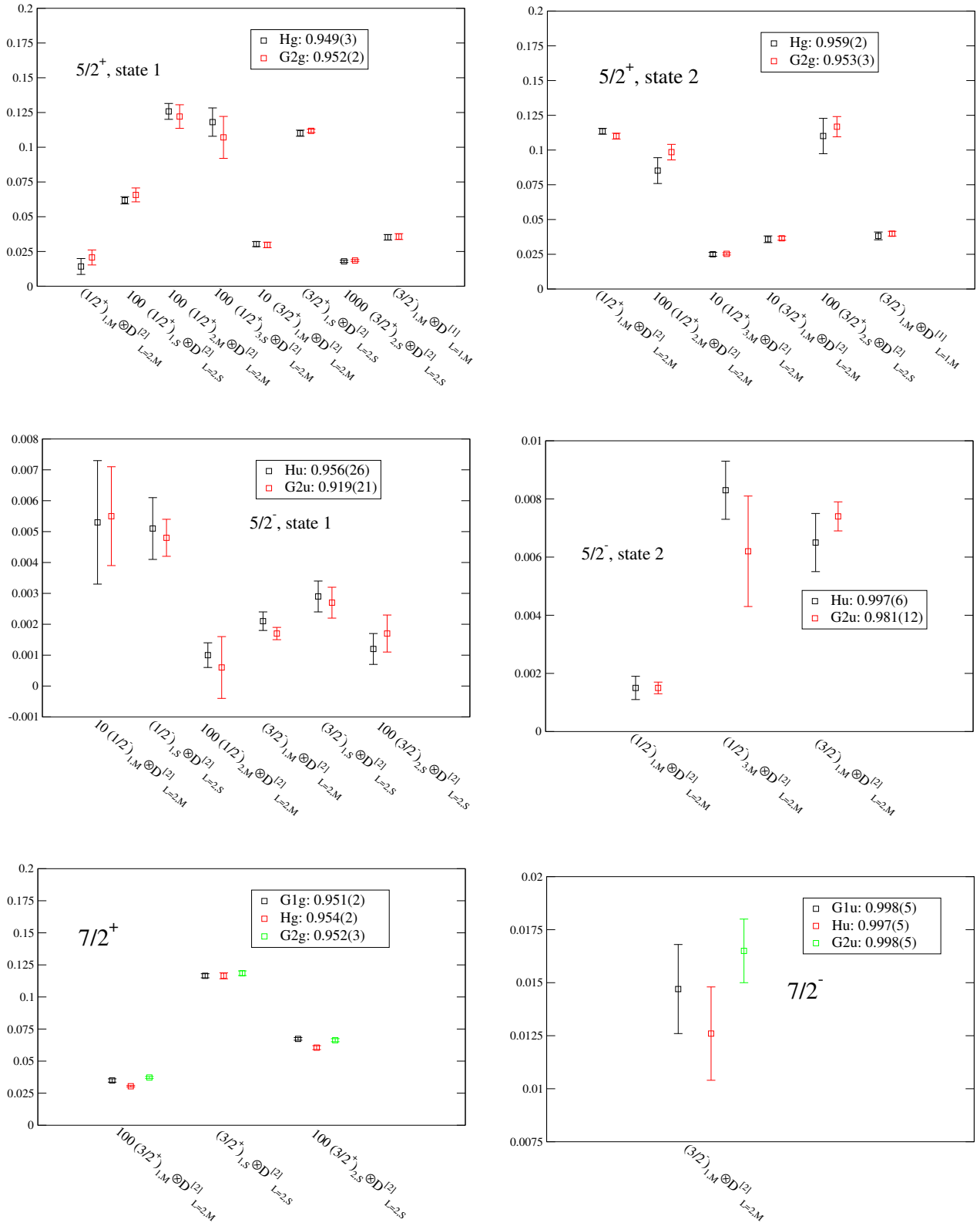

FIG. 6: A selection of Z-values for states conjectured to be identified with $J^P = \frac{5}{2}^+$ (top two plots), $\frac{5}{2}^-$ (middle two plots), $\frac{7}{2}^+$ (bottom left) and $\frac{7}{2}^-$ (bottom right). Operators in consideration, which overlap to these states, are mentioned at the bottom of each plot. Z-values obtained for a given operator, but from different irreps, are found to be consistent or very close to each other which helps to identify the spin of a given state. Some operators are scaled so the set can all be shown on a single panel. These rescalings are indicated by numbers in front of the operator labels.

In Ref. [36], a simple experiment was carried out to provide a crude estimate of the systematic uncertainty due to $\mathcal{O}(a)$ discretisation artefacts. The charm quark action is discretised using an action that removes the $\mathcal{O}(a_s)$ effects at the tree-level. To assess if radiative corrections to the co-efficient of the improvement term in the charm-quark action could lead to significant changes in physical predictions, a second calculation was carried out after the co-efficient was boosted from the tree-level $c_s = 1.35$ to $c_s = 2$. In the charmonium study, the shift in the mass difference between the two lightest states, the η_c and J/Ψ was found to be 45 MeV. For the energy difference $m_{\Omega_{ccc}} - 3/2 m_{\eta_c}$, a very similar shift is observed in the lowest few states, indicating a similar scale of uncertainty in this calculation. The higher lying states do not show any statistically significant difference between the two charm quark actions. Here the factor of $\frac{3}{2}$ corrects for the different number of valence charm quarks in a triply-charmed baryon and the η_c meson. Figure 7 shows this alongside other published lattice data, which use a different discretisation and so have distinct artefacts. Our result for this quantity is consistent with Refs. [29–32], but is not consistent with Ref. [28].

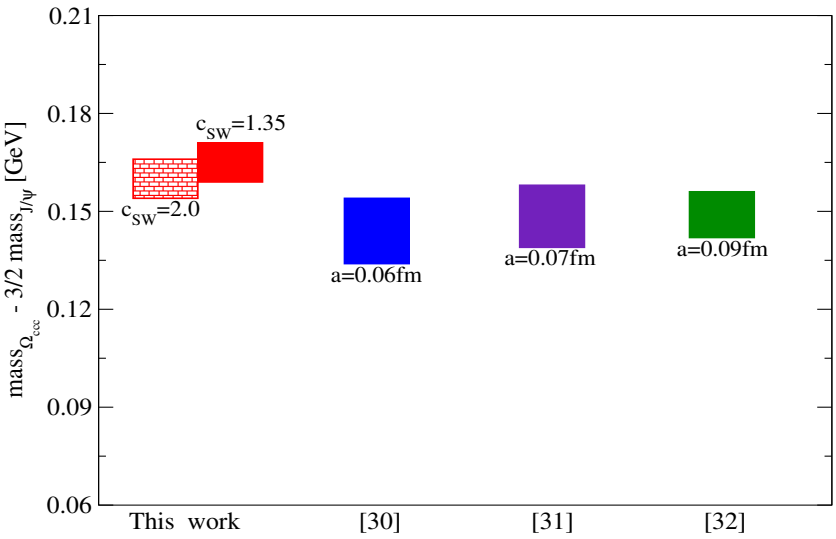

FIG. 7: Mass splitting of the ground state of $J^P = \frac{3}{2}^+$ Ω_{ccc} from J/ψ meson. A factor 3/2 is multiplied with J/ψ mass to account for the difference in the number of charm quarks in baryons and mesons. This mass splitting mimics the binding energy of the ground state Ω_{ccc}. Results of this mass splitting from this work (red boxes) are compared with those obtained from other lattice calculations [29–32].

III. RESULTS

In this section we present our results spectra for spins up to $\frac{7}{2}$ and for both parities. Results for the extracted masses as well as mass splittings from charmonia states are presented. Various spin dependent energy splittings between the extracted states are also considered along with similar splittings at light, strange as well as bottom quark masses. Results for the light and strange quark masses are from Ref. [40] and bottom quark results are from Ref. [48].

Due to systematic uncertainty in the determination of the charm quark mass parameter in the lattice action, it is preferable to compare energy splittings between states that reduce the impact of these uncertainties. This also lessens the effect of ambiguity in the scale setting procedure. In Ref. [36], the quark mass was determined by ensuring the ratio of masses of the η_c meson and Ω-baryon took its physical value. Consequently for this study, the spectrum is presented relative to the reference scale of $\frac{3}{2} m_{\eta_c}$, where the factor of $\frac{3}{2}$ corrects for the different number of valence charm quarks in triply-charmed baryon and charmonium states. This subtracted spectrum is presented in Figure 8 and tabulated in Table V. Boxes with thicker borders correspond to those with a greater overlap onto operators proportional to the field strength tensor as discussed in the previous section and which might consequently be hybrid states. The states inside the pink ellipses have relatively large overlap with non-relativistic operators and should thus be well described in a quark model. An analysis of the spectrum using only the non-relativistic operators is presented in the right panel of Figure 8. The main difference between the two panels is the absence of spin-5/2 and spin-7/2 negative parity states when only operators that couple to the dominant spin components for heavy quarks moving non-relativistically. In Ref. [48], triply-bottom baryons were studied. The main difference with the set of operators used in that calculation is the inclusion of the non-relativistic hybrid operators in this work, which provides access to higher excited states.

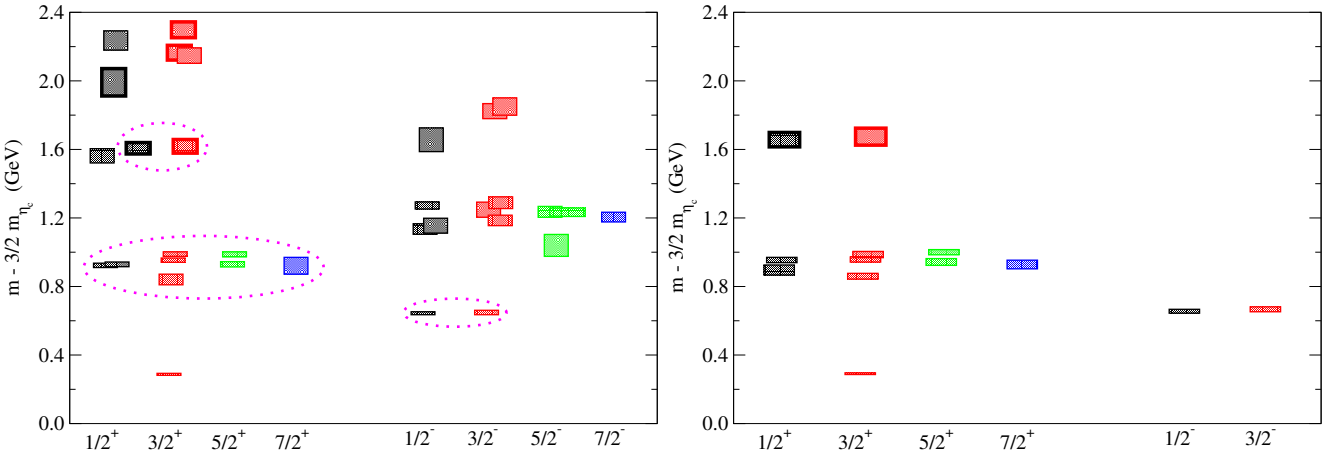

FIG. 8: Spin identified spectra of triply-charmed baryons with respect to $\frac{3}{2}m_{\eta_c}$. The boxes with thick borders corresponds to the states with strong overlap with hybrid operators. The states inside the pink ellipses are those with relatively large overlap to non-relativistic operators.

$\frac{1}{2}^+$	$\frac{3}{2}^+$	$\frac{5}{2}^+$	$\frac{7}{2}^+$	$\frac{1}{2}^-$	$\frac{3}{2}^-$	$\frac{5}{2}^-$	$\frac{7}{2}^-$
0.923(13)	0.287(6)	0.930(15)	0.921(49)	0.644(9)	0.648(13)	1.040(64)	1.205(28)
0.929(14)	0.841(31)	0.988(15)		1.136(31)	1.186(31)	1.233(25)	
1.563(33)	0.954(13)			1.155(43)	1.248(44)	1.234(24)	
1.607(42)	0.989(13)			1.273(21)	1.289(34)	1.236(32)	
1.992(80)	1.618(40)			1.656(69)	1.823(44)		
2.236(56)	2.147(46)				1.850(51)		
	2.165(43)						
	2.298(46)						

TABLE V: Spin identified spectra of triply-charmed baryons with respect to $\frac{3}{2}m_{\eta_c}$ (that is $m_{\Omega_{ccc}} - \frac{3}{2}\ m_{\eta_c}$.)

In the lowest positive-parity band and the two lowest negative-parity bands the number of states for each spin agrees with the expectation given in Table II. In that table, the number of states is presented for operator built from up to two derivatives and this corresponds to the number allowed by $SU(6) \times O(3)$ symmetry. In this picture for $N_D = 0$, only one state with $J^P = \frac{3}{2}^+$ is expected. For $N_D = 1$ the expected quantum numbers are $J^P = \frac{1}{2}^-$ and $J^P = \frac{3}{2}-$ and for $N_D = 2$, a set of positive parity states with a range of spins from $\frac{1}{2}$ to $\frac{5}{2}$ is predicted with multiple states appearing for the lower spins. This pattern is clearly seen in the spectrum determined by this calculation. This agreement of the number of low lying states between the lattice spectra obtained in this work and the expectations based on non-relativistic quark spins implies a clear signature of $SU(6) \times O(3)$ symmetry in the spectra. Such $SU(6) \times O(3)$ symmetric nature of spectra was also observed in Ref. [40]. As was pointed out in Ref. [40], it is not meaningful to interpret the higher excited states in terms of $SU(6) \times O(3)$ symmetry. The reasons behind this are following : firstly, we did not include non-relativistic operators with three derivatives and secondly for higher excited states it is expected that the relativistic operators generally overlaps more with these states. For negative parity it is also not possible to identify a state with strong hybrid content because it is not clear how the relative importance of all the relevant operators overlapping to that state will change in the presence of non-relativistic operators having three or more number of derivatives.

A. Valence quark mass dependence of energy splittings

Spin-dependent splittings between the triply-flavoured baryons provide an insight into interactions between three confined quarks with the same mass. We consider now the dependence of these splittings on the mass of the valence quarks.

As presented in Table II, operators with increasing numbers of gauge-covariant derivatives (which can correspond to

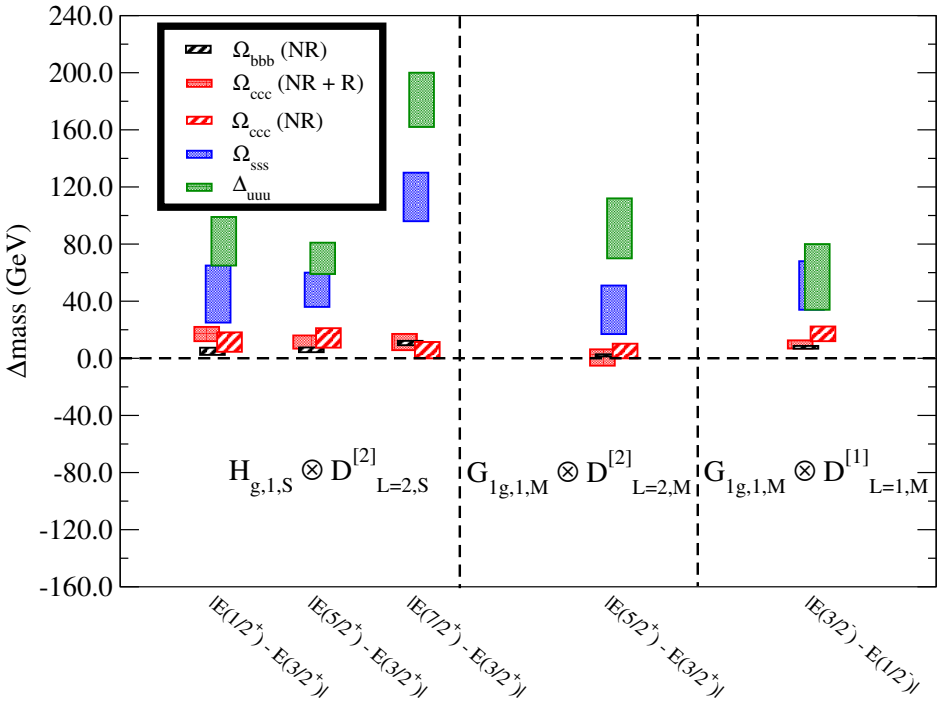

FIG. 9: Energy splittings between states with same L and S values, starting from light to heavy baryons. For Ω_{bbb}, results are with only non-relativistic operators [48]; for Ω_{ccc}, results from relativistic and non-relativistic as well as only non-relativistic operators are shown, and for light and strange baryons results are with relativistic and non-relativistic operators [40]. These results are obtained from fitting the jackknife ratio of the correlators which helps to get smaller errorbar in splittings. The left column is for the states with $D = 2, S = \frac{3}{2}$ and $L = 2$. The symbol $H_{g,1,S}$ refers to the first embedding of irrep H_g in the totally symmetric Dirac spin combination, while $D^{[2]}_{L=2,S}$ refers to spatial projection operators with two derivatives in a totally symmetric combination, and with orbital angular momentum two. Similarly, the middle column is for the states with $D = 2, S = \frac{1}{2}$ and $L = 2$. Here irrep is G_{1g} and both Dirac and derivative are in a mixed symmetric combination. In the right column these negative parity states have $D = 1, S = \frac{1}{2}$ and $L = 1$. Here again irrep is G_{1g} and both Dirac and derivative are in a mixed symmetric combination.

non-zero orbit angular momentum in a quark model) create states with numerous values of total spin J. For example, we construct flavour (F) decuplet states with $D = 2, S = \frac{3}{2}$ and $L = 2$ with the combination $\{10F_S \otimes (S)_S \otimes (D)_S\}$, where S in the subscript stands for symmetric combinations, as defined in Ref. [38]. In this way of construction we get four quantum numbers with $J^P = \frac{1}{2}^+, \frac{3}{2}^+, \frac{5}{2}^+$ and $\frac{7}{2}^+$. In the heavy quark limit the spin-orbit interaction vanishes since the interaction term is inversely proportional to the square of the heavy quark mass. States corresponding to quantum numbers ($|L, S, J^P\rangle \equiv |2, \frac{3}{2}, \frac{1}{2}^+\rangle, |2, \frac{3}{2}, \frac{3}{2}^+\rangle, |2, \frac{3}{2}, \frac{5}{2}^+\rangle$ and $|2, \frac{3}{2}, \frac{7}{2}^+\rangle$) will thus be degenerate in the heavy quark limit. Similarly, two states with quantum numbers $J^P = \frac{1}{2}^-$ and $\frac{3}{2}^-$ with $L = 1$ and $S = \frac{1}{2}$ will also be degenerate in the heavy quark limit. In Figure 9 we plot absolute values of energy differences between energy levels which originate from the spin-orbit interaction of the following (L, S) pairs : $(2, \frac{3}{2}$ –in the left column), $(2, \frac{1}{2}$ –in the middle column) and $(1, \frac{1}{2}$ –in the right column). We plot these spin-orbit energy splittings at various quark masses corresponding to following triple-flavoured baryons : Δ_{uuu}, Ω_{sss}, Ω_{ccc} and Ω_{bbb}. We identified the states with these (L, S) pairs by finding the operators which incorporate these pairs and which have major overlaps to these states. These energy differences are obtained from the ratio of jackknifed correlators, which in general, reduce errorbars by cancelling correlation of these correlators. For bottom baryons we use data from Ref. [48] and for light and strange baryon results from Ref. [40] are used.

It should be noticed that energy levels shown for bottom baryons are obtained from only non-relativistic operators [48]. For charm baryons we show results from the full set of operators (including relativistic operators) as well as from only non-relativistic operators, and for light and strange baryons the splittings results are obtained also with the full set operators. In some cases we find that the inclusion of the relativistic operators increase errorbars. As one can observe that the degeneracy between these states is more or less satisfied both for bottom and charm quarks. However, data with higher statistics is necessary to identify the breaking of this degeneracy at charm quark. We will address this issue in future. For $\Delta(uuu)$ and $\Omega(sss)$ some of these splittings are non-zero. This is expected because of

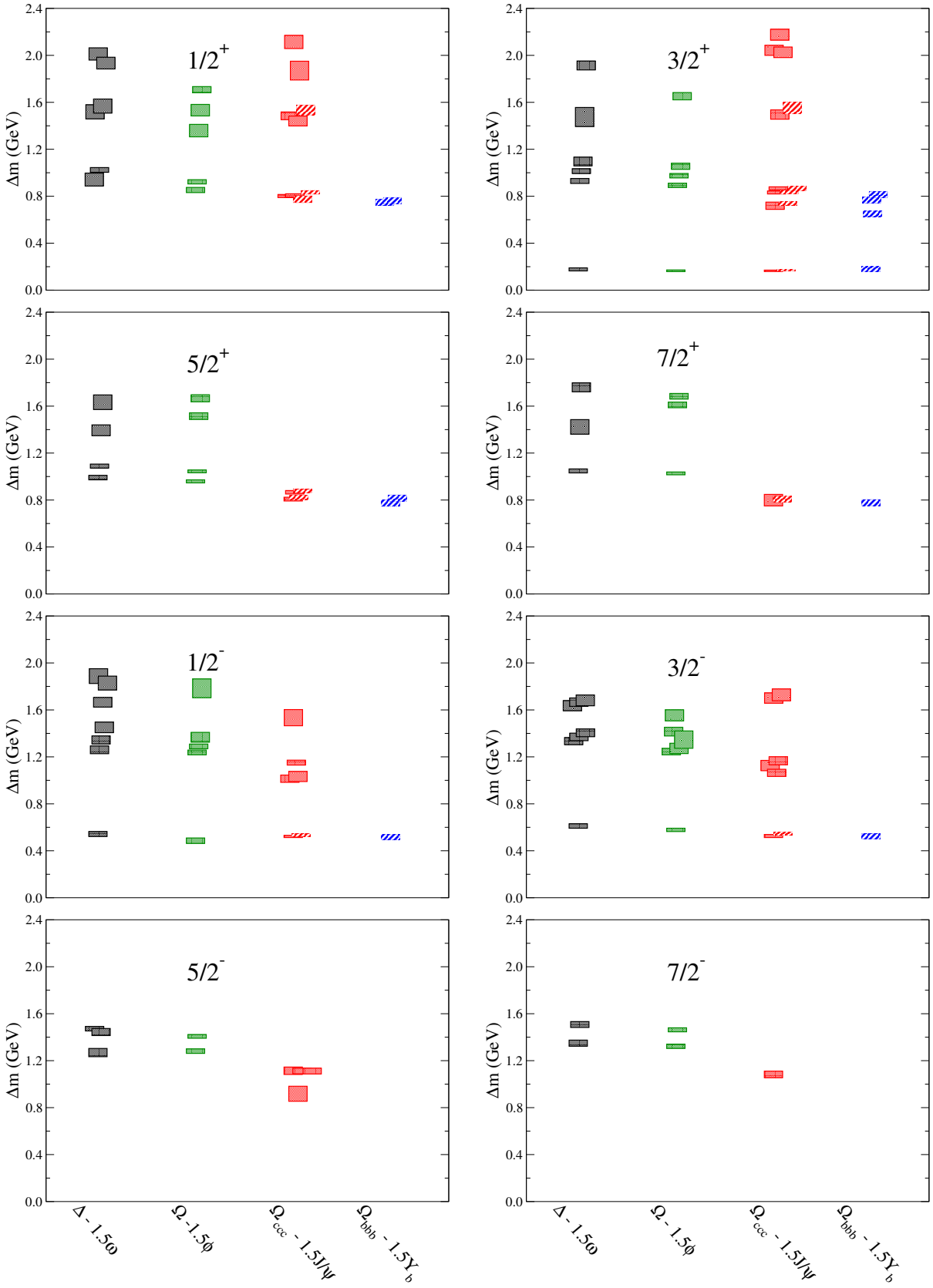

FIG. 10: Energy splittings of triply-flavoured baryons at various quark masses (u to b $\rightarrow$ left to right) from the respective isoscalar vector meson (irrep T_1^{--}) ground state. Top four figures are for positive parity states and bottom four are for negative parity states respectively. A factor 3/2 is multiplied with isoscalar vector meson masses to account for the difference in the number of charm quarks in baryons and mesons. For charm quark, results are from this work, while for light and strange quark results are from Ref. [40] and those for bottom quark are from Ref. [48]. The zebra-shaded boxes are the results obtained by using only non-relativistic operators.

the presence of the light quark masses in the denominator of the spin-orbit interaction which enhance these splittings.

We also compared how energy splittings change between light and heavy baryons. Some of these, such as the hyperfine splitting, vanish in the heavy quark limit while others become constant. However, most splittings tend to be higher at lighter quark masses where relativistic effects are prominent. We determined the energy difference between the triply-flavoured baryons with respect to the isoscalar vector mesons with two constituents of the same flavour. To make a comparison which is independent of the quark mass in the heavy quark limit, we subtract $\frac{3}{2}$ of the vector meson mass, where this factor simply takes account of the difference in the number of charm quarks between baryons and mesons. Specifically we consider following splittings: $m_{\Delta_{uuu}} - \frac{3}{2}\, m_{\omega_{\bar{u}u}}$, $m_{\Omega_{sss}} - \frac{3}{2}\, m_{\phi_{\bar{s}s}}$, $m_{\Omega_{ccc}} - \frac{3}{2}\, m_{J/\psi_{\bar{c}c}}$ and $m_{\Omega_{bbb}} - \frac{3}{2}\, m_{\Upsilon_{\bar{b}b}}$. Figure 10 shows these splittings for positive and negative parity states at varying quark masses from the light u, d quarks up to the b-quark mass. For $\Delta^{++}(uuu)$ and Ω_{sss} baryons, results are from Ref. [40], while for Ω_{bbb}, we use results from Ref. [48]. The zebra-shaded boxes are the results obtained using only non-relativistic operators. These splittings mimic the binding energies of triple-flavoured states and thus it is interesting to compare these as a function of quark masses. In Figure 11 we plot these splittings, for the ground-state and a few excitations as a function of the square of the pseudoscalar meson masses. Notice that most of the splittings in various spin parity channels decrease with quark mass. In the heavy quark limit, naively one can expand the mass of a heavy hadron, with n heavy quarks, as $M_{H_{nq}} = n\, m_Q + A + B/m_Q + \mathcal{O}(1/m_Q{}^2)$ [50]. We expect that these energy splittings can also be expressed in the form $a + b/m_Q$ and similarly in the heavy quark limit with $a + b/m_{ps}$. Note this form is not expected to be valid for light hadrons. Using this function we fitted the data obtained for $m_{\Omega_{bbb}} - \frac{3}{2}\, m_{\Upsilon_{\bar{b}b}}$, $m_{\Omega_{ccc}} - \frac{3}{2}\, m_{J/\psi_{\bar{c}c}}$ and $m_{\Omega_{sss}} - \frac{3}{2}\, m_{\phi_{\bar{s}s}}$. Because of the very different behaviour in the chiral limit, the light quark point, $m_{\Delta_{uuu}} - \frac{3}{2}\, m_{\omega_{\bar{u}u}}$ is excluded from the fit. For the cases where data for the bottom quark are not available (mainly for negative parity cases), fitting is done using only the two data at charm and strange masses. While there is no good reason for the heavy-quark inspired functional form to model the data at the strange quark mass, a good fit is still found. We also extrapolate fit results to lighter pion masses and observe that for many cases they pass through the light quark points though those points are *not* included in these fits. The fitted results for the parameters a and b are tabulated in Table VI. However, as mentioned before, one should not use this extrapolation to get splittings at lighter quark masses as is evident in many cases where data points fall significantly below the fit. It is worth noting that that the energy splittings for the spin-$\frac{3}{2}^+$ and spin-$\frac{1}{2}^-$ ground states are almost constant even when varying the quark mass from light to bottom. In fact, we observe better fit with a constant term for these splittings.

State	a	b	χ^2/DOF	State	a	b	χ^2/DOF
$\frac{1}{2}^+$	773 (16)	59 (22)	1.8	$\frac{1}{2}^-$	511 (12)		0.9
$\frac{1}{2}^+$	758 (16)	117 (19)	0.4	$\frac{1}{2}^-$	963 (31)	193 (27)	
$\frac{3}{2}^+$	168 (9)	-2.0 (9)	0.5	$\frac{3}{2}^-$	513 (14)	45 (15)	0.08
$\frac{3}{2}^+$	170 (5)		0.4				
$\frac{3}{2}^+$	640 (22)	179 (21)	0.56	$\frac{3}{2}^-$	1089 (30)	109 (20)	
$\frac{3}{2}^+$	765 (17)	149 (21)	1.2				
$\frac{3}{2}^+$	805 (12)	177 (21)	0.18				
$\frac{5}{2}^+$	760 (17)	140 (16)	0.01	$\frac{5}{2}^-$	954 (61)	230 (50)	
$\frac{5}{2}^+$	807 (17)	167 (15)	0.15	$\frac{5}{2}^-$	1021 (26)	271 (26)	
$\frac{7}{2}^+$	739 (17)	201 (16)	0.7	$\frac{7}{2}^-$	1009 (30)	220 (27)	

TABLE VI: Fitted values of the parameters a and b for the heavy quark expansion of the mass difference $\Delta m_H = a + b/m_{ps}$. Left side is for positive parity and the right side is for negative parity states. Colour coding for these states are corresponding to Figure 11. We do not quote χ^2/DOF for the cases where there are only two data points (*i.e.*, data points are not available at the bottom quark).

IV. CONCLUSIONS

In this work, we present results from the first non-perturbative calculation on the excited state spectroscopy of the triply-charmed baryons with spin up to 7/2. This system is the baryonic analogue of charmonium, which has been central to understanding more about the phenomenology of the strong force. Calculations were performed using anisotropic lattice QCD with a background of $2 + 1$ dynamical light quarks with pion mass of about 390 MeV in a finite volume with extent of approximately 1.9 fm where the temporal and spatial spacings were $a_t = 0.0351(2)$ fm

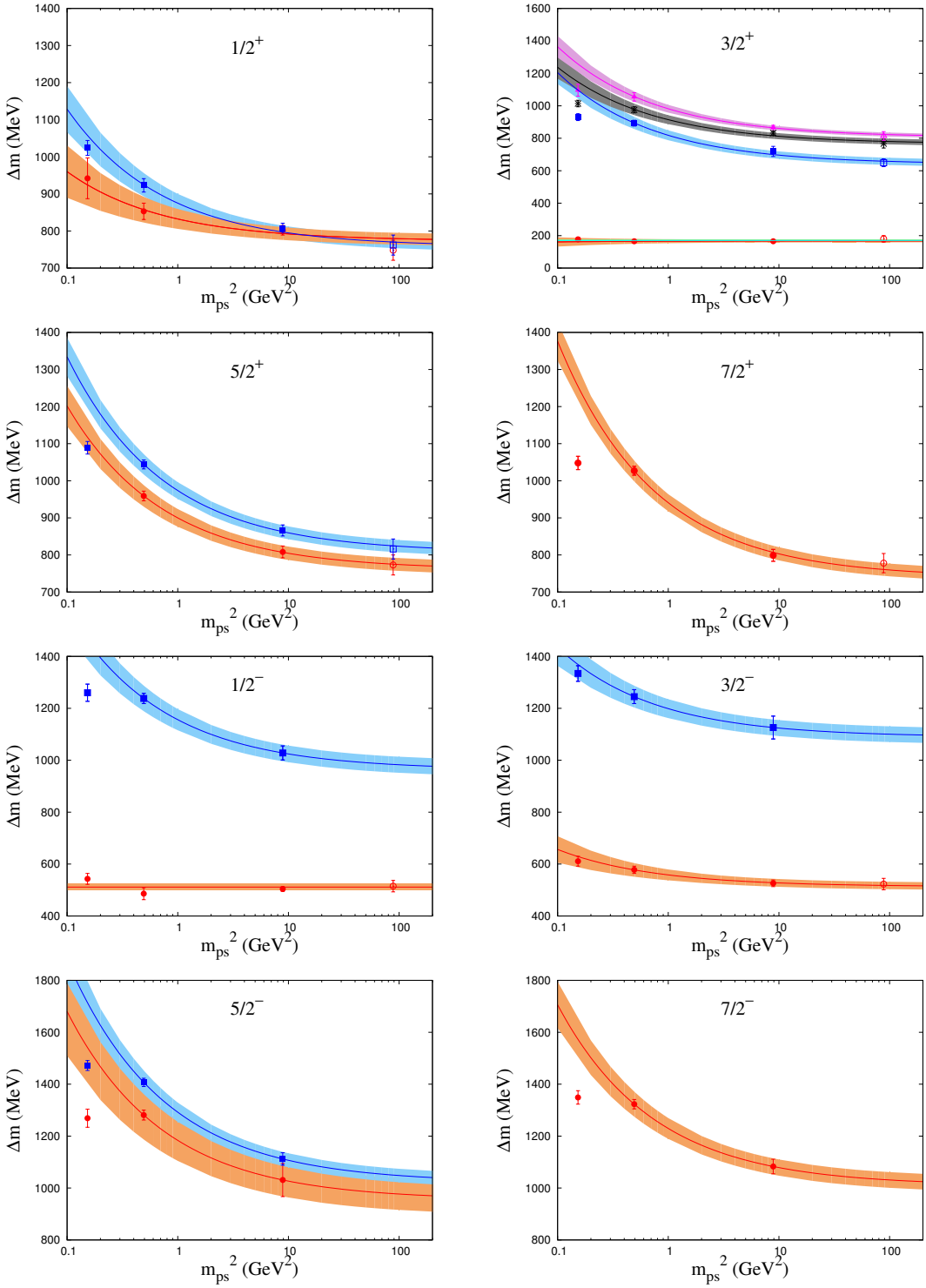

FIG. 11: Energy splittings of a few triple-flavoured baryons (labeled by different symbols and colours) from isoscalar vector meson (irrep T_1^{--}) ground state are plotted against the square of the pseudoscalar masses. Top four figures are for positive parity and bottom four are for negative parity baryons respectively. This energy splitting mimics the binding energy and considering that these plots show the dependence of binding energies of these states as a function of quark mass. We fit this dependence with a form $a + b/m_{ps}$ (please see text for details).

and $a_s \sim 0.12$ fm respectively. The systematic uncertainties due to chiral, continuum and final volume extrapolations

have not been explored here and those will be addressed in future.

Using the distillation smearing technique to make use of the variational method, we extracted the spectrum of triply-charmed baryons comprising a total of 18 states, including spin up to 7/2. We use a large set of continuum operators which can be classified according to the irreducible representation of $SU(3)_F$ flavour and which transform according to good total angular momentum in the continuum. Angular momenta are realized by including up to two covariant derivatives in creation operators. Similar to earlier work, we observe approximate rotational symmetry for these operators at the scale of hadrons. By using this symmetry and calculating overlap factors of various operators to energy eigenstates and then comparing those over irreps we are able to extract states reliably with spin up to 7/2. We also observe that there is strong mixing between states created by non-relativistic non-hybrid and relativistic non-hybrid type operators but comparatively weaker mixing between those created by hybrid and non-hybrid type operators. Additional suppression of mixing is seen for non-relativistic operators with given J but with different L and S compared to those with the same J, L and S. However, this suppression is not present for relativistic operators.

The main results are shown in Figure 8. As in Ref. [40], we also find bands of states with alternating parities and increasing energies. Beside identifying the spin of a state we are also able to decode the structure of operators leading to that state : whether constructed by relativistic, non-relativistic, hybrids, non-hybrid types or a mixture of them all. However, for negative parity states and highly excited positive parity states, this identification is not possible since we do not include operators with more than two derivatives which will contribute to these states and so will change the relative contribution from various operators leading to such states. Similar to light and strange baryon spectra [40], we also find the number of extracted states of each spin in the three lowest-energy bands and the number of quantum numbers expected based on weakly broken $SU(6) \times O(3)$ symmetry agree perfectly, *i.e.,* the triply-charmed baryon spectra remarkably resemble the expectations of quantum numbers from quark model [51–53]. Even the inclusion of non-relativistic hybrid operators does not spoil this agreement for positive parity states. However, with the inclusion of relativistic operators which contribute more to the higher excited states it is expected that this band structure will not be followed. That is what we also observe for the higher excited states. However, it is to be noted that we have not used any multi-hadron operators in this calculation. Inclusion of those operators, particularly those involving light quarks, may affect some of the above conclusions, though to a lesser extent than their influence in the light hadron spectra.

Various energy splittings, including splittings due to spin-orbit coupling, are also evaluated for these baryons and those are compared with similar splittings obtained at light, strange as well as bottom quark masses. While the data at charm quark mass (for Ω_{ccc}) is from this work, those for light and strange quark masses (for Δ_{uuu} and Ω_{sss} baryons) are taken from Ref. [40] and bottom quark results (for Ω_{bbb}) are from Ref. [48]. The energy splittings between baryons due to spin-orbit coupling vanish at the heavy quark limit. To check this degeneracy we identify the states with same L and S values from overlap factors of various operators and find that the spin-orbit energy degeneracy between these states are more or less satisfied both for bottom and charm quarks. However, for a few cases they are non-zero at lighter quark masses. More precise data is necessary to check the breaking of this degeneracy at the charm quark mass.

The energy splitting of the triply-charmed baryon spectrum, from the isoscalar vector meson (irrep T_1^{--}) ground state is also evaluated. These splittings are compared with similar ones obtained at other quark masses. For the splitting, which mimics the binding energy of these states, significant quark mass dependence is observed for ground as well as for first few excited states, except for the $J^P = 3/2^+$ and $J^P = 1/2^-$ ground states. These splittings can be modelled with a form $a + b/m_{\rm ps}$ to show their expected quark mass dependence which assumes they will tend to a constant in the heavy quark limit, It is interesting to note this form gives a good fit with data at bottom, charm as well as strange masses. For some of them, we observe that the extrapolated fit lines pass through the light quark data points even when they are not included in the fit.

V. ACKNOWLEDGMENTS

We thank our colleagues within the Hadron Spectrum Collaboration. NM also likes to thank S. Datta for useful discussions. Chroma [54] and QUDA [55, 56] were used to perform this work on the Gaggle and Brood clusters of the Department of Theoretical Physics, Tata Institute of Fundamental Research and at Lonsdale cluster maintained by the Trinity Centre for High Performance Computing funded through grants from Science Foundation Ireland (SFI), at the SFI/HEA Irish Centre for High-End Computing (ICHEC) and at Jefferson Laboratory under the USQCD Initiative and the LQCD ARRA project. Gauge configurations were generated using resources awarded from the U.S. Department of Energy INCITE program at the Oak Ridge Leadership Computing Facility at Oak Ridge National Laboratory, the NSF Teragrid at the Texas Advanced Computer Center and the Pittsburgh Supercomputer Center, as well as at Jefferson Lab. MP acknowledges support from the Trinity College Dublin Indian Research Collaboration Initiative and the Council of Scientific and Industrial Research, India for financial support through the Shyama Prasad

Mukherjee Fellowship; NM acknowledges support from Department of Science and Technology, India under grant No. DST-SR/S2/RJN-19/2007; RGE acknowledges support from support from U.S. Department of Energy contract DE-AC05-06OR23177, under which Jefferson Science Associates, LLC manages and operates Jefferson Laboratory. This research was supported by the European Union under Grant Agreement number 238353 (ITN STRONGnet).

[1] The Review of Particle Physics : J. Beringer et al. (Particle Data Group), Phys. Rev. D86, 010001 (2012)
[2] M. Mattson *et al.* [SELEX Collaboration], Phys. Rev. Lett. **89**, 112001 (2002) [hep-ex/0208014].
[3] A. Ocherashvili *et al.* [SELEX Collaboration], Phys. Lett. B **628**, 18 (2005) [hep-ex/0406033].
[4] J. S. Russ [SELEX Collaboration], hep-ex/0209075.
[5] B. Aubert *et al.* [BABAR Collaboration], Phys. Rev. D **74**, 011103 (2006) [hep-ex/0605075].
[6] R. Chistov *et al.* [BELLE Collaboration], Phys. Rev. Lett. **97**, 162001 (2006) [hep-ex/0606051].
[7] J. D. Bjorken, FERMILAB-CONF-85/69, Is the ccc a New Deal for Baryon Spectroscopy?, Int. Conf. on Hadron Spectroscopy, College Park, MD, Apr. 1985; Unpublished Draft, Estimates of Decay Branching Ratios for Hadrons Containing Charm and Bottom Quarks, July 22, 1986; Unpublished Draft, Masses of Charm and Strange Baryons, Aug. 13, 1986.
[8] Y. -Q. Chen and S. -Z. Wu, JHEP **1108**, 144 (2011) [Erratum-ibid. **1109**, 089 (2011)] [arXiv:1106.0193 [hep-ph]].
[9] M. A. Gomshi Nobary and R. Sepahvand, Nucl. Phys. B **741**, 34 (2006) [hep-ph/0508115].
[10] N. Brambilla, S. Eidelman, B. K. Heltsley, R. Vogt, G. T. Bodwin, E. Eichten, A. D. Frawley and A. B. Meyer *et al.*, Eur. Phys. J. C **71**, 1534 (2011) [arXiv:1010.5827 [hep-ph]].
[11] W. Roberts and M. Pervin, Int. J. Mod. Phys. A **23**, 2817 (2008) [arXiv:0711.2492 [nucl-th]].
[12] J. Vijande, H. Garcilazo, A. Valcarce and F. Fernandez, Phys. Rev. D **70**, 054022 (2004) [hep-ph/0408274].
[13] A. P. Martynenko, Phys. Lett. B **663**, 317 (2008) [arXiv:0708.2033 [hep-ph]].
[14] S. Migura, D. Merten, B. Metsch and H. -R. Petry, Eur. Phys. J. A **28**, 41 (2006) [hep-ph/0602153].
[15] B. Silvestre-Brac, Few Body Syst. **20**, 1 (1996).
[16] P. Hasenfratz, R. R. Horgan, J. Kuti and J. M. Richard, Phys. Lett. B **94**, 401 (1980).
[17] N. Brambilla, A. Pineda, J. Soto and A. Vairo, Rev. Mod. Phys. **77**, 1423 (2005) [hep-ph/0410047].
[18] N. Brambilla, A. Vairo and T. Rosch, Phys. Rev. D **72**, 034021 (2005) [hep-ph/0506065].
[19] N. Brambilla, J. Ghiglieri and A. Vairo, Phys. Rev. D **81**, 054031 (2010) [arXiv:0911.3541 [hep-ph]].
[20] F. J. Llanes-Estrada, O. I. Pavlova and R. Williams, Eur. Phys. J. C **72**, 2019 (2012) [arXiv:1111.7087 [hep-ph]].
[21] J. M. Flynn, E. Hernandez and J. Nieves, Phys. Rev. D **85**, 014012 (2012) [arXiv:1110.2962 [hep-ph]].
[22] Y. Jia, JHEP **0610**, 073 (2006) [hep-ph/0607290].
[23] J. -R. Zhang and M. -Q. Huang, Phys. Lett. B **674**, 28 (2009) [arXiv:0902.3297 [hep-ph]].
[24] Z. -G. Wang, Commun. Theor. Phys. **58**, 723 (2012) [arXiv:1112.2274 [hep-ph]].
[25] X. -H. Guo, K. -W. Wei and X. -H. Wu, Phys. Rev. D **78**, 056005 (2008) [arXiv:0809.1702 [hep-ph]].
[26] J. G. Korner, M. Kramer and D. Pirjol, Prog. Part. Nucl. Phys. **33**, 787 (1994) [hep-ph/9406359].
[27] T. -W. Chiu and T. -H. Hsieh, Nucl. Phys. A **755**, 471 (2005) [hep-lat/0501021].
[28] C. Alexandrou, J. Carbonell, D. Christaras, V. Drach, M. Gravina and M. Papinutto, Phys. Rev. D **86**, 114501 (2012) [arXiv:1205.6856 [hep-lat]].
[29] R. A. Briceno, H. -W. Lin and D. R. Bolton, Phys. Rev. D **86**, 094504 (2012) [arXiv:1207.3536 [hep-lat]].
[30] S. Basak, S. Datta, M. Padmanath, P. Majumdar and N. Mathur, PoS LATTICE **2012**, 141 (2012) [arXiv:1211.6277 [hep-lat]] and PoS LATTICE 2013.
[31] S. Durr, G. Koutsou and T. Lippert, Phys. Rev. D **86**, 114514 (2012) [arXiv:1208.6270 [hep-lat]].
[32] Y. Namekawa *et al.* [PACS-CS Collaboration], Phys. Rev. D **87**, 094512 (2013) [arXiv:1301.4743 [hep-lat]].
[33] J. J. Dudek, R. G. Edwards, M. J. Peardon, D. G. Richards and C. E. Thomas, Phys. Rev. D **82**, 034508 (2010) [arXiv:1004.4930 [hep-ph]].
[34] J. J. Dudek, R. G. Edwards, M. J. Peardon, D. G. Richards and C. E. Thomas, Phys. Rev. Lett. **103**, 262001 (2009) [arXiv:0909.0200 [hep-ph]].
[35] J. J. Dudek, R. G. Edwards, M. J. Peardon, D. G. Richards and C. E. Thomas, Phys. Rev. D **83**, 071504 (2011) [arXiv:1011.6352 [hep-ph]].
[36] L. Liu *et al.* [Hadron Spectrum Collaboration], JHEP **1207**, 126 (2012) [arXiv:1204.5425 [hep-ph]].
[37] G. Moir, M. Peardon, S. M. Ryan, C. E. Thomas and L. Liu, arXiv:1301.7670 [hep-ph].
[38] R. G. Edwards, J. J. Dudek, D. G. Richards and S. J. Wallace, Phys. Rev. D **84**, 074508 (2011) [arXiv:1104.5152 [hep-ph]].
[39] J. J. Dudek and R. G. Edwards, Phys. Rev. D **85**, 054016 (2012) [arXiv:1201.2349 [hep-ph]].
[40] R. G. Edwards, N. Mathur, D. G. Richards and S. J. Wallace, arXiv:1212.5236 [hep-ph].
[41] R. G. Edwards, B. Joo and H. -W. Lin, Phys. Rev. D **78**, 054501 (2008) [arXiv:0803.3960 [hep-lat]].
[42] H. -W. Lin *et al.* [Hadron Spectrum Collaboration], Phys. Rev. D **79**, 034502 (2009) [arXiv:0810.3588 [hep-lat]].
[43] M. Peardon *et al.* [Hadron Spectrum Collaboration], Phys. Rev. D **80**, 054506 (2009) [arXiv:0905.2160 [hep-lat]].
[44] A. X. El-Khadra, A. S. Kronfeld and P. B. Mackenzie, Phys. Rev. D **55**, 3933 (1997) [hep-lat/9604004].
[45] E. Follana *et al.* [HPQCD and UKQCD Collaborations], Phys. Rev. D **75**, 054502 (2007) [hep-lat/0610092].
[46] C. Michael, Nucl. Phys. B **259**, 58 (1985).
[47] M. Luscher and U. Wolff, Nucl. Phys. B **339**, 222 (1990).

[48] S. Meinel, Phys. Rev. D **85**, 114510 (2012) [arXiv:1202.1312 [hep-lat]].
[49] J. J. Dudek, R. G. Edwards, N. Mathur and D. G. Richards, Phys. Rev. D **77**, 034501 (2008) [arXiv:0707.4162 [hep-lat]].
[50] E. E. Jenkins, Phys. Rev. D **54**, 4515 (1996) [hep-ph/9603449].
[51] O. W. Greenberg, Phys. Rev. Lett. **13**, 598 (1964).
[52] N. Isgur and G. Karl, Phys. Lett. B **72**, 109 (1977).
[53] N. Isgur and G. Karl, Phys. Rev. D **18**, 4187 (1978).
[54] R. G. Edwards *et al.* [SciDAC and LHPC and UKQCD Collaborations], Nucl. Phys. Proc. Suppl. **140**, 832 (2005) [hep-lat/0409003].
[55] M. A. Clark, R. Babich, K. Barros, R. C. Brower and C. Rebbi, Comput. Phys. Commun. **181**, 1517 (2010) [arXiv:0911.3191 [hep-lat]].
[56] R. Babich, M. A. Clark and B. Joo, arXiv:1011.0024 [hep-lat].